Spin dynamics of YH_2 and YD_2

J. T. Markert and R. M. Cotts
Laboratory of Atomic and Solid State Physics, Cornell University, Ithaca, New York 14853-2501
(Received 20 April 1987)

The properties of cross relaxation between dipolar and rotating-frame Zeeman nuclear-spin subsystems in the metal hydride YH_2 and deuteride YD_2 are examined using pulsed NMR spin-locking measurements in single resonance experiments on the ^{89}Y spin system. A thermodynamic model is presented to describe the spin dynamics. Observed equilibrium values of the ^{89}Y magnetization are described in terms of the magnetic heat capacities of the subsystems and provide a measure of the second moment of the nonresonant spins. Measured cross-relaxation spectra are described in terms of proton dipolar fluctuations; a comparison with numerically calculated spectra is presented. Additional insight into the strength and spectral width of the cross relaxation is provided by comparing the isotopes YH_2 and YD_2. The calculated spectra decay exponentially with the ^{89}Y rotating-frame angular frequency, with characteristic widths of 38.6 μs for YH_2 and 1.003 ms for YD_2. In addition to the quasiequilibrium cross-relaxation processes, large transient oscillations in Zeeman-dipolar order are observed and discussed. Finally, results from spin-echo measurements indicate that transverse decay processes are describable by the same fluctuation spectrum used in the description of cross relaxation.

I. INTRODUCTION

Experiments utilizing cross relaxation between rare (or weak) and abundant (or strong) nuclei have proven quite important,[1-6] especially for high-sensitivity measurements of weak nuclei. Typically, such cross relaxation is achieved in a double-resonance experiment under the Hartmann-Hahn condition,[1] where two rf fields are employed to match the precession frequencies of the two-spin species. In this paper, cross-relaxation phenomena are investigated by directly observing the weak spin ^{89}Y in a *single* resonance experiment. Yttrium dihydride provides an ideal spin system: both ^{89}Y and ^{1}H are spin $\frac{1}{2}$, 100% abundant isotopes, yet their gyromagnetic ratios differ by a large factor, $\gamma_Y/\gamma_H \approx 1/20$, so that the characteristic phenomena associated with cross relaxation between weak and abundant nuclei are clearly manifested.

After a discussion of experimental details in Sec. II, a spin temperature description is emphasized in Sec. III. A thermodynamic model is described there, providing a framework for the rest of the paper. Section IV deals with the long-time behavior of the magnetization. There, the equilibrium eventually achieved by the yttrium-hydrogen spin system is analyzed primarily using energy-conservation considerations. The intermediate time scale during which the cross relaxation occurs is the subject of Sec. V; a detailed theory based upon that of Demco, Tegenfeldt, and Waugh[7] (hereafter abbreviated DTW) provides predictions of the spectral densities for the cross relaxation process. Section VI discusses the early time behavior of the magnetization, which is characterized by dramatic transient oscillations. In Sec. VII, the discussion of the spin system is extended to the case of zero applied rotating field.

II. EXPERIMENTAL DETAILS

Samples of YH_2 and YD_2 were prepared from high-purity Ames Laboratory yttrium. Spark-source mass spectroscopy indicated extremely low concentrations (0.1–1 ppm) of typical paramagnetic impurities. Hydrogen concentrations were determined to within 2% by monitoring the change in pressure upon exposing the metal to a known volume of H_2 gas; absorption of H_2 proceeds exothermically. All other sample handling and preparation was performed in an inert atmosphere to prevent oxidation of the metal. Sample concentrations were verified by weighing the hydrided metal. After grinding, the metal powder was sealed and annealed at 450 °C for 30 h to insure uniform concentration; particle sizes in the range 44–74 μm (200–325 mesh) were then selected by sieving. The small particle size was chosen to allow good rf field penetration; for the same reason, the metal powder was then mixed with quartz powder and resealed in glass sample tubes. X-ray powder patterns exhibited a single fcc dihydride phase with a lattice constant of 5.20 Å, in agreement with other investigators.[8-11]

The NMR spin-locking experiments were performed using a conventional superheterodyne spectrometer with an intermediate frequency of 160 MHz which has been described elsewhere.[12] The magnetization was measured by monitoring the amplitude of the free-induction decay following the spin-locking pulse; these free-induction decays were recorded on a Nicolet 4094 digital oscilloscope. Repetition periods of approximately 30 s were typical; signal-averaging periods of up to 6 h for a given magnetization curve were required to obtain reasonable signal-to-noise ratios.

The external field of 5.9 T was provided by an Oxford

Instruments persistent-mode superconducting solenoid; the corresponding ^{89}Y resonant frequency was 12.2 MHz. The solenoid was equipped with an Oxford MD4 cryostat and DTC2 temperature controller, which was stable and accurate to within 1 K in the temperature range utilized for these experiments, 100–200 K. As discussed below, this temperature range was low enough to ensure sufficiently weak-lattice coupling during the pulse sequences, but high enough to permit reasonable repetition rates and to avoid skin depth problems.

The rotating field H_1 was calibrated by application of a π or $n\pi$ pulse, where n is an integer, and detecting a null in the free-induction decay; the accuracy of the values of H_1 reported here is approximately 3%. Values of H_1 in the range 1–30 G ($f_1=0.2$–6 kHz) were used in the experiments. The homogeneity of H_1 is limited by two factors: the skin depth of the metal particles and coil geometry. The coil geometry chosen was dictated by a compromise between H_1 homogeneity and sample filling factor; the latter consideration is necessary to maximize signal strength. Skin-depth problems were negligible by virtue of the precautions mentioned above; this was confirmed by the observed Curie temperature dependence of the apparent magnetization throughout the temperature range of the experiment. Deviation from Curie behavior occurred below ~ 70 K, where the resistivity of the metal particles became sufficiently low to prevent full rf field penetration.

III. THERMODYNAMICS

Van Vleck[13] first described the conditions under which Curie's law could be extended to include nonequilibrium magnetizations. Even when not in equilibrium with the lattice, the nuclear magnetization M can be characterized by a spin temperature T according to

$$M=\frac{CH}{T} , \tag{1}$$

where C is the Curie constant, $C=N\gamma^2\hbar^2 I(I+1)/3k_B$. The spin temperature is then a measure of the extent of preferential alignment of the spins parallel to the field H.[14]

All of the results of the three subsequent sections are from ordinary spin-locking experiments performed on the ^{89}Y nuclei in YH_2 and YD_2. In such an experiment, one begins with the large Curie magnetization M_0, corresponding to equilibrium at the lattice temperature T_L in a large, static external field H_0. After tipping the magnetization 90°, a small rotating field H_1 is immediately applied *parallel* to it, thus establishing a large magnetization parallel to a small field H_1. In terms of a spin-temperature description,[15] the magnetization has been artificially cooled to an initial temperature T_i much different from the lattice temperature:

$$M_0=\frac{CH_1}{T_i} ,$$

where

$$T_i=\frac{H_1}{H_0}T_L . \tag{2}$$

Since in this experiment H_1/H_0 is in the range 10^{-3}–10^{-5}, a very low initial spin temperature has been achieved; correspondingly, a large nonequilibrium value of the rotating frame Zeeman energy has been created.

The large Zeeman energy will tend to relax toward its much lower equilibrium value, provided a coupling for energy transfer to some other reservoir is present. It is the detailed time evolution of the magnetization from its initial nonequilibrium value which is of interest here. Hereafter, the resonant ^{89}Y spins in YH_2 and YD_2 will also be referred to as the I spins; the nonresonant ^1H (or ^2D) spins will also be referred to as the S spins.

Figure 1 depicts the energy reservoirs relevant to this experiment. Eventually, the Zeeman energy could be transferred to the lattice via some standard route, labeled by time constant T_{IL}. However, this coupling is quite weak for the temperatures at which the measurements were performed, 100–200 K. At these temperatures, there is no appreciable motion of the protons (rigid lattice regime) and thus no relaxation by translational diffusion. The remaining electronic coupling is quite weak; measurements indicate $T_{IL}\approx 10$ s.

A more strongly coupled energy reservoir involving quanta comparable to those of the rotating-frame Zeeman energy exists, namely, the dipolar energy of alignment of protons along their local fields. The strongly coupled protons frequently undergo mutual spin flips, due to the flip-flop terms of the form $S_i^+S_j^-$ in their dipolar Hamiltonian. These mutual flips conserve the large proton Zeeman energy, but avail small changes in dipolar energy. An I-S dipolar term in the Hamiltonian provides the coupling between the S-spin dipolar energy and the I-spin Zeeman energy. Equivalently, one can view the proton mutual spin flips as producing field fluctuations at the yttrium sites; these fluctuations will cause relaxation because they have appreciable spectral density at the rotating frame frequency, $\omega_1=\gamma_I H_1$.

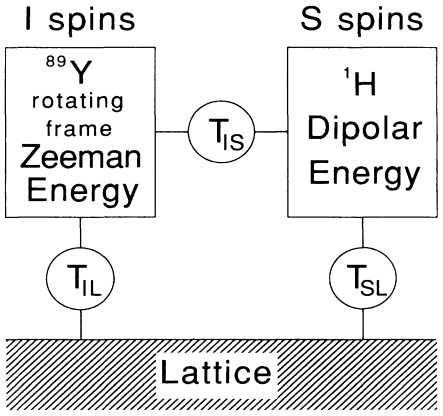

FIG. 1. Thermodynamic model for the spin-locking experiment. The ^{89}Y rotating-frame Zeeman energy is coupled to the ^1H dipolar energy by the I-S interaction. Electronic coupling to the lattice for either reservoir is weak.

The quantitative form of the dipolar fluctuation spectrum is the subject of the Sec. V. Before that, the equilibrium achieved between the Zeeman and dipolar subsystems will be examined; this depends only on the relative heat capacities of the two reservoirs. It should be mentioned that since the time scale of the cross relaxation is in the millisecond range, while, as mentioned above, the lattice coupling is much weaker, the four subsequent sections assume with validity that the Zeeman and dipolar energies are isolated from the lattice. Thus, for example, the following discussion of Zeeman-energy–dipolar-energy equilibrium implies a quasiequilibrium, on a time scale short compared with relaxation to the lattice.

IV. EQUILIBRIUM

To examine the long-time (equilibrium) behavior of the magnetization, a number of similar approaches[2–4,16–18] utilizing conservation of energy and a spin-temperature description have been employed. One can start with the system Hamiltonian in the rotating frame:

$$\mathcal{H}=\mathcal{H}_{Z_I}+\mathcal{H}^0_{d_{II}}+\mathcal{H}^0_{d_{IS}}+\mathcal{H}^0_{d_{SS}} . \tag{3}$$

The first term

$$\mathcal{H}_{Z_I}=-\gamma_I\hbar H_1\sum_i I_{xi} \tag{4}$$

represents the rotating-frame Zeeman energy of the I spins. The secular (time-independent) terms of dipole-dipole interactions are

$$\mathcal{H}^0_{d_{II}}=-\sum_{i,j} b_{ij}(3I_{zi}I_{zj}-\mathbf{I}_i\cdot\mathbf{I}_j) , \tag{5}$$

$$\mathcal{H}^0_{d_{IS}}=-\sum_{i,j} B_{ij}I_{xi}S_{zj} , \tag{6}$$

$$\mathcal{H}^0_{d_{SS}}=-\sum_{i,j} A_{ij}(3S_{zi}S_{zj}-\mathbf{S}_i\cdot\mathbf{S}_j) , \tag{7}$$

where the coefficients are given by

$$b_{ij}=-\tfrac{1}{2}\gamma_I^2\hbar\frac{(1-3\cos^2\theta_{ij})}{r_{ij}^3} , \tag{8}$$

$$B_{ij}=\gamma_I\gamma_S\hbar\frac{(1-3\cos^2\theta_{ij})}{r_{ij}^3} , \tag{9}$$

$$A_{ij}=-\tfrac{1}{2}\gamma_S^2\hbar\frac{(1-3\cos^2\theta_{ij})}{r_{ij}^3} . \tag{10}$$

It is the last term, $\mathcal{H}^0_{d_{SS}}$, which comprises the large S-spin dipolar reservoir. The Zeeman energy of the S spins has been neglected; it essentially remains in equilibrium with the lattice, playing no part in the experiment under consideration.

To calculate the expectation value of the energy, the density matrix is used in the high-temperature approximation:

$$\rho=\frac{\exp(-\mathcal{H}/k_BT)}{\mathrm{Tr}[\exp(-\mathcal{H}/k_BT)]}\approx\left[1-\frac{\mathcal{H}}{k_BT}\right] , \tag{11}$$

where it will be assumed that all traces are suitably normalized to $\mathrm{Tr}\{1\}=(2I+1)^{N_I}(2S+1)^{N_S}$. Adopting the spin-temperature description, the state of each spin subsystem is identified by a temperature. The initial state of the system can thus be described by a density matrix of the form

$$\rho_i=1-\frac{1}{k_BT_i}\mathcal{H}_{Z_I}-\frac{1}{k_BT_L}(\mathcal{H}^0_{d_{II}}+\mathcal{H}^0_{d_{IS}}+\mathcal{H}^0_{d_{SS}}) . \tag{12}$$

Here, $T_i=(H_1/H_0)T_L$ and the lattice temperature can be written $T_L=C_IH_0/M_0$, as discussed above.

The coupling which provides the thermal mixing is the subject of Sec. V. Here, it is assumed that the two reservoirs eventually reach an equilibrium state characterized by a common final spin temperature, $T_f=C_IH_1/M_f$, where M_f is the equilibrium value of the spin-locked magnetization. Thus the density matrix for the final state is

$$\rho_f=1-\frac{1}{k_BT_f}(\mathcal{H}_{Z_I}+\mathcal{H}^0_{d_{II}}+\mathcal{H}^0_{d_{IS}}+\mathcal{H}^0_{d_{SS}}) . \tag{13}$$

Conservation of the total spin energy then requires

$$E_i=\mathrm{Tr}\{\rho_i\mathcal{H}\}=\mathrm{Tr}\{\rho_f\mathcal{H}\}=E_f . \tag{14}$$

Evaluating the various traces leads immediately to

$$\frac{M_f}{M_0}=\frac{H_1^2+(H_1/H_0)[\frac{1}{3}(\Delta H_{II}^{(I)})^2+(\Delta H_{IS}^{(I)})^2+\frac{1}{3}(C_S/C_I)(\Delta H_{SS}^{(S)})^2]}{H_1^2+\frac{1}{3}(\Delta H_{II}^{(I)})^2+(\Delta H_{IS}^{(I)})^2+\frac{1}{3}(C_S/C_I)(\Delta H_{SS}^{(S)})^2} , \tag{15}$$

or, more simply,

$$\frac{M_f}{M_0}\approx\frac{H_1^2}{H_1^2+\frac{1}{3}(C_S/C_I)(\Delta H_{SS}^{(S)})^2} , \tag{16}$$

where the dipolar traces have been expressed in terms of various second moments with conventional[19] definitions:

$$(\Delta H_{II}^{(I)})^2=\tfrac{3}{4}\gamma_I^2\hbar^2I(I+1)\sum_i\frac{(1-3\cos^2\theta_{ij})^2}{r_{ij}^6} , \tag{17}$$

$$(\Delta H_{IS}^{(I)})^2=\tfrac{1}{3}\gamma_S^2\hbar^2S(S+1)\sum_i\frac{(1-3\cos^2\theta_{ij})^2}{r_{ij}^6} , \tag{18}$$

$$(\Delta H_{SS}^{(S)})^2=\tfrac{3}{4}\gamma_S^2\hbar^2S(S+1)\sum_i\frac{(1-3\cos^2\theta_{ij})^2}{r_{ij}^6} . \tag{19}$$

The sums are with respect to a typical spin j. The second term in the numerator of Eq. (15) has been neglected in Eq. (16), since here $H_1/H_0\approx10^{-4}$. The last term in the denominator of Eq. (15) clearly dominates

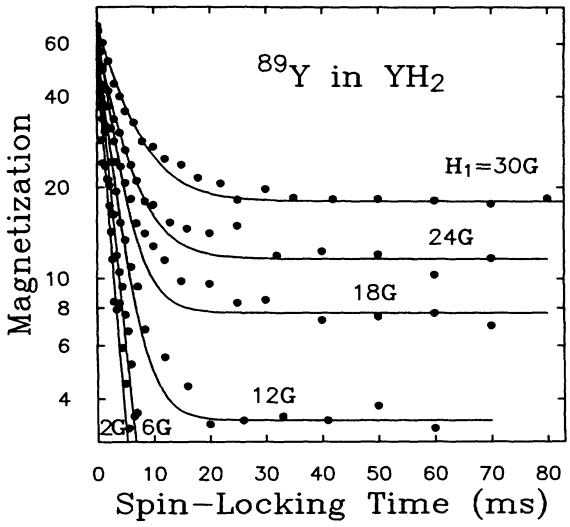

FIG. 2. Yttrium spin-locked magnetization plotted as a function of spin-locking time for polycrystalline YH_2. Data for several values of rotating field H_1 are shown. The initial decay is a result of thermal mixing of ^{89}Y Zeeman energy with ^{1}H dipolar energy; the long-time plateau indicates that the two reservoirs have equilibrated at a common final spin temperature.

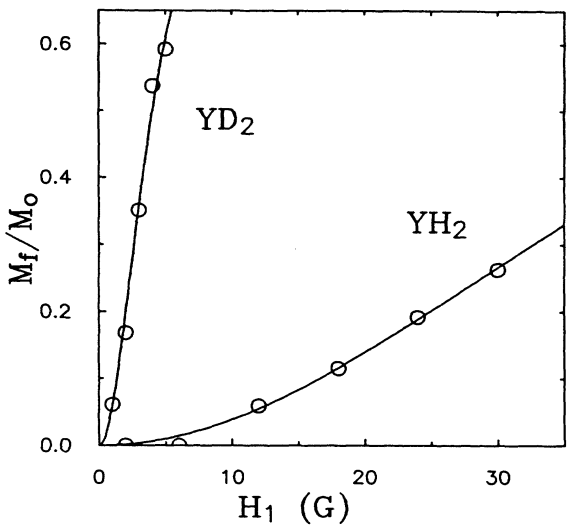

FIG. 4. The ratio of final to initial magnetization extracted from Figs. 2 and 3 and plotted as a function of rotating field H_1 (open circles). The solid lines are fits to Eq. (16), from which the second moments of the nonresonant S spins appearing in Table I are obtained.

the two terms preceeding it, because the S-S second moment is augmented by a factor equal to the ratio of the Curie constants of the two reservoirs,

$$\frac{C_S}{C_I}=\frac{N_S\gamma_S^2 S(S+1)}{N_I\gamma_I^2 I(I+1)}\ , \tag{20}$$

which equals 833 for protons in YH_2.

Data for the time dependence of the spin-locked ^{89}Y magnetization in YH_2 and YD_2 are shown in Figs. 2 and 3, respectively. The magnetization initially decays as the nonequilibrium ^{89}Y rotating-frame Zeeman energy is converted into dipolar energy. Then, at long times, the magnetization approaches a constant value, indicating that the two reservoirs have reached equilibrium at a common final spin temperature. Since the heat capacity of the dipolar reservoir is constant, while the heat capacity of the Zeeman reservoir is proportional to H_1^2, the final magnetization increases with H_1, as predicted by Eq. (16).

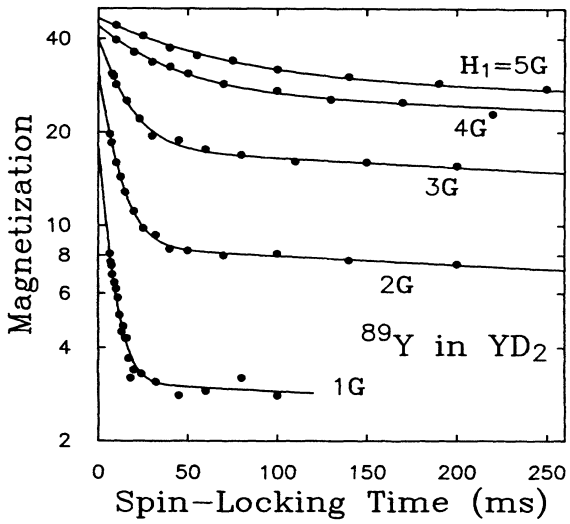

FIG. 3. Similar to Fig. 2, but for polycrystalline YD_2.

To make a quantitative comparison with theory, the ratio of final to initial magnetization has been extracted from Figs. 2 and 3 and plotted in Fig. 4 as a function of H_1. The solid curves in Fig. 4 are fits to Eq. (16); from each of these fits, the second moments of the nonresonant S spins can be obtained. These values are listed in Table I, together with the theoretical values, which can be calculated from Eq. (19). For the theoretical calculation, stoichiometric YH_2 (YD_2) was assumed, with only (and full) tetrahedral occupancy. As is implicit in Eqs. (17)–(19), only the dipolar contribution to the second moments is included in the calculation.

Quite acceptable agreement is found in the case of the hydride, considering the scatter in the data and a variety

TABLE I. Second moments for the nonresonant S spins, ^{1}H and ^{2}D, in YH_2 and YD_2. Experimental values were obtained from the data of Fig. 4 by fitting to Eq. (16). Theoretical values were obtained from a powder average of Eq. (19).

	$(\Delta H_{SS}^{(S)})^2$ (G^2)	
	YH_2	YD_2
Experiment	9.0+−0.8	1.02+−0.09
Theory	9.7	0.61

of experimental considerations (e.g., H_1 inhomogeneity). For the deuteride, however, a large discrepancy is apparent. The deuteron, however, is a spin-1 nucleus; as such, it experiences a quadrupole interaction due to random electric field gradients caused by distortions of its ideally cubic environment. Such distortions are presumably the result of partial ($\sim 5\%$) octahedral occupancy and the concurrent tetrahedral vacancies, which are characteristic of the yttrium-hydrogen system.[20–22] The existence of quadrupole broadening increases the second moment $(\Delta H_{SS}^{(S)})^2$ and thus increases the heat capacity of the S-spin system. To verify that this additional contribution to the deuteron second moment was indeed present, the rigid lattice line shape for the deuteron resonance was obtained by Fourier transform spectroscopy. This yielded the value $(\Delta H_{SS}^{(S)})^2=0.99$ G^2, in excellent agreement with the 1.02 G^2 obtained from the cross-relaxation equilibrium. This agreement is strong evidence to suggest that in the case of a small quadrupole splitting (here, ~ 0.4 G^2), the quadrupole energy is in close contact with the deuteron dipolar energy, thus enlarging the total spin energy reservoir.

Thus simple energy-conservation considerations in the framework of a spin-temperature description adequately describe the equilibrium behavior of the spin-locked ^{89}Y magnetization. The same spin-temperature picture will be utilized in subsequent sections to discuss the time-dependent phenomena involved in the approach to equilibrium.

V. CROSS-RELAXATION RATE

To begin discussion of the time evolution of the initial nonequilibrium ^{89}Y magnetization, this section will primarily examine the cross-relaxation rate for energy transfer between ^{89}Y rotating-frame Zeeman energy and ^{1}H dipolar energy. As was previously mentioned, the mechanism for such transfer exists in the I-S dipolar coupling; when a pair of strongly coupled protons undergo a mutual spin flip (S-S interaction), the resulting field fluctuations at a nearby I-spin site have appreciable spectral density at low ($\sim\omega_1$) frequencies, and thus can contribute to the relaxation of the I spin.

To motivate the discussion, let us rewrite the Hamiltonian of Eq. (3) in the form

$$\mathcal{H}=\mathcal{H}_{Z_I}+\mathcal{H}_{d_{SS}}^0+\mathcal{H}_{d_{IS}}^0\equiv\mathcal{H}_I+\mathcal{H}_S+\mathcal{H}_p \ , \tag{21}$$

where the $\mathcal{H}_{d_{II}}^0$ term has been omitted, since it is much smaller than the $\mathcal{H}_{d_{IS}}^0$ term, which itself is a small perturbation, denoted $\mathcal{H}_p$. An inverse spin temperature, $\beta=1/k_B T$, for each of the two reservoirs may be written as

$$\beta_I=\frac{\mathrm{Tr}\{\rho\mathcal{H}_I\}}{\mathrm{Tr}\{\mathcal{H}_I^2\}}=\frac{\langle\mathcal{H}_I\rangle}{\mathrm{Tr}\{\mathcal{H}_I^2\}}$$

and

$$\beta_S=\frac{\mathrm{Tr}\{\rho\mathcal{H}_S\}}{\mathrm{Tr}\{\mathcal{H}_S^2\}}=\frac{\langle\mathcal{H}_S\rangle}{\mathrm{Tr}\{\mathcal{H}_S^2\}} \ . \tag{22}$$

Notice that conservation of energy, $d/dt(\langle\mathcal{H}_I\rangle+\langle\mathcal{H}_S\rangle)=0$, implies that

$$\frac{d}{dt}(\epsilon\beta_I+\beta_S)=0$$

where

$$\epsilon=\frac{\mathrm{Tr}\{\mathcal{H}_I^2\}}{\mathrm{Tr}\{\mathcal{H}_S^2\}}=\frac{C_I H_1^2}{\frac{1}{3}C_S(\Delta H_{SS}^{(S)})^2} \ . \tag{23}$$

Thermodynamic equations describing the relaxation of the instantaneous I-spin inverse temperature toward the instantaneous S-spin inverse temperature have been derived by DTW (Ref. 7) using an orthogonal operator expansion and projection operator techniques. This theory has also been reviewed in detail by Mehring.[23] The decay process is characterized by a time constant T_{IS}.

$$\frac{d}{dt}\beta_I=-\frac{1}{T_{IS}}(\beta_I-\beta_S) \ . \tag{24}$$

Equation (24) defines T_{IS}; a coupled equation then follows from Eq. (23):

$$\frac{d}{dt}\beta_S=-\frac{\epsilon}{T_{IS}}(\beta_S-\beta_I) \ . \tag{25}$$

The rigorous DTW theory involves no explicit spin-temperature assumptions,[23] and thus describes the time evolution of the expectation values in Eq. (22) quite generally. The quantity $1/T_{IS}$ in Eqs. (24) and (25) is given by[7,23]

$$\begin{aligned}\frac{1}{T_{IS}}&=M_{IS}^2\int_0^t d\tau\cos(\omega_1\tau)C(\tau)\\&\approx M_{IS}^2\int_0^\infty d\tau\cos(\omega_1\tau)C(\tau) \ ,\end{aligned} \tag{26}$$

where the last equality is valid for times $t\gg\tau_c$, τ_c being a correlation time characteristic of the normalized correlation function, $C(\tau)$, described below. Here, $\omega_1=\gamma_I H_1$ and M_{IS}^2 is the second moment of the I-S dipole-dipole interaction expressed in angular frequency units, i.e., $M_{IS}^2=\gamma_I^2(\Delta H_{IS}^{(I)})^2$, where $(\Delta H_{IS}^{(I)})^2$ was given in Eq. (18). The correlation function is found[7,23] to have the form

$$C(\tau)=\frac{\mathrm{Tr}\left[\left[\sum_i B_i S_{zi}\right]\exp\left[\frac{-i\mathcal{H}_S\tau}{\hbar}\right]\left[\sum_i B_i S_{zi}\right]\exp\left[\frac{i\mathcal{H}_S\tau}{\hbar}\right]\right]}{\mathrm{Tr}\left[\left[\sum_i B_i S_{zi}\right]^2\right]} \ , \tag{27}$$

where

$$B_i=\gamma_I\gamma_S\hbar\frac{(1-3\cos^2\theta_i)}{r_i^3} \tag{28}$$

as in Eq. (9), but now written with respect to a typical I spin. It is conventional to approximate $C(\tau)$ by a Lorentzian function of τ; this assumption has a great deal of experimental confirmation[3] in that the measured spectral density of cross-relaxation decay rates, $J_d(\omega)$, has been observed to be an exponential function of ω over many decades, and the two are, by definition, related by a Fourier transform,

$$\frac{1}{T_{IS}}=M_{IS}^2J_d(\omega_1)=M_{IS}^2\int_0^\infty d\tau\cos(\omega_1\tau)C(\tau)\ . \tag{29}$$

The Lorentzian approximation is also justified by an expansion[7] of Eq. (27) in powers of τ, which is quite tedious. With this assumption one can write

$$C(\tau)=\frac{1}{1+\tau^2/\tau_c^2}\ , \tag{30}$$

$$J_d(\omega_1)=\frac{\pi}{2}\tau_c\exp(-\omega_1\tau_c)\ , \tag{31}$$

where τ_c can then be evaluated simply by equating the one term quadratic in τ in the expansion of Eq. (27) with that of Eq. (30). Upon evaluating the traces, one obtains the result

$$\frac{1}{\tau_c^2}=\tfrac{1}{3}S(S+1)\frac{\sum_{i<j}A_{ij}^2(B_i-B_j)^2}{\sum_i B_i^2}\ , \tag{32}$$

where B_i and A_{ij} have been defined in Eqs. (28) and (10), respectively. From this form of τ_c two observations should be made. First, the term $A_{ij}^2\propto 1/r_{ij}^6$ highlights the dependence of the effectiveness in contributing to relaxation of any pair of protons on the strength of the coupling between them. Thus, nearest-neighbor proton pairs will undergo mutual spin flips more frequently than less proximate pairs.[18] Second, the term $(B_i-B_j)^2$ indicates that to produce a field fluctuation at an yttrium site, the proton pair under consideration must be situated asymmetrically with respect to that site. A mutual flip between two protons positioned symmetrically about an yttrium nucleus (i.e., $B_i=B_j$) produces no net change in dipolar field at that site, and thus does not contribute to relaxation.

The time scale for which the second equality in Eq. (26) is valid is determined by τ_c, which can be calculated using Eq. (32). Upon numerically averaging over crystal orientation, one obtains the values $\bar{\tau}_c=38.6$ μs (YH_2) and $\bar{\tau}_c=1.003$ ms (YD_2). For $t\gg\tau_c$, Eq. (26) indicates that $1/T_{IS}$ is independent of time; combining Eqs. (29) and (31) gives

$$\frac{1}{T_{IS}}=\frac{\pi}{2}M_{IS}^2\tau_c\exp(-\omega_1\tau_c)\ . \tag{33}$$

For such a time-independent $1/T_{IS}$, the solution to Eqs. (24) and (25) is simply

$$\beta_I(t)=\beta_I(\infty)+[\beta_I(0)-\beta_I(\infty)](1-e^{-(1+\epsilon)t/T_{IS}})\ , \tag{34}$$

where ϵ is given by Eq. (23). The equilibrium value

$$\beta_I(\infty)=\frac{\beta_S(0)+\epsilon\beta_I(0)}{1+\epsilon} \tag{35}$$

is determined solely by the initial conditions and the ratio of heat capacities, ϵ, as was seen in Sec. IV. Indeed, since $\beta_S(0)=(H_1/H_0)\beta_I(0)\approx 0$, Eq. (35) asserts that $\beta_I(\infty)/\beta_I(0)=\epsilon/(1+\epsilon)$, which is identical to Eq. (16).

To extract the cross-relaxation rate, $1/T_{IS}$, the data of Figs. 2 and 3 were fitted to the exponential form of Eq. (34). Note that actual decay rates will be larger than the conventionally defined quantity $1/T_{IS}$ by the factor $(1+\epsilon)$. Data for $t<8\tau_c$ were omitted to incorporate the $t\gg\tau_c$ requirement discussed above. Data for those shorter times will be discussed in Sec. VI. The results are plotted in Fig. 5. To compare with the theory described above, and in order to accommodate the polycrystalline nature of the powdered metal samples used, an angular average is necessary. Because of the three different angles contained in each of the fourth-moment-like terms in Eq. (32), an analytical averaging is not possible. Therefore, a numerical calculation was performed: the lattice sums of Eq. (32) were calculated for 155 magnetic field directions in one-sixteenth of 4π steradians; a frequency-dependent rate was calculated for each direction. Appropriate angular averaging thus permitted the calculation of the powder average decay of the net magnetization (cf. Sec. VII). Because of the anisotropy of the lattice sums, the decay of the net magnetization is necessarily somewhat nonexponential. Rather than take the *average rate,* which overemphasizes the more quickly decaying crystal orientations, the full net

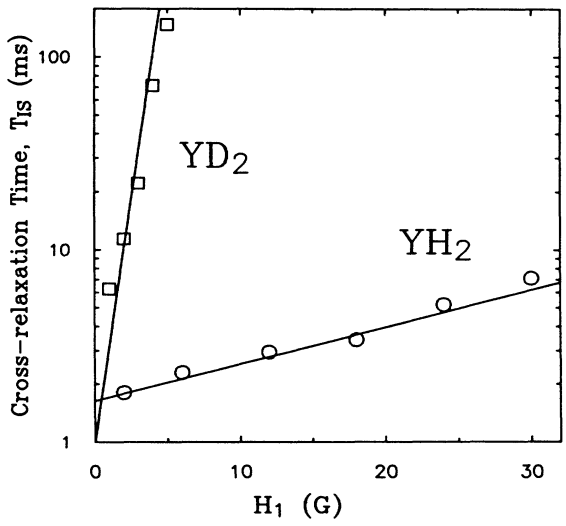

FIG. 5. Cross-relaxation spectra. The cross-relaxation times T_{IS} for YH_2 (circles) and YD_2 (squares) were obtained from the data of Figs. 2 and 3, respectively, by fitting to Eq. (34). The lines shown are the theoretical predictions of Sec. V, generated with no adjustable parameters.

magnetization decay was fit to a single exponential. This provided the theoretical powder average decay constant T_{IS} to which the experimental data is compared.

The theoretical predictions are shown as the solid lines in Fig. 5. It should be emphasized that these theoretical exponential spectral densities are calculated with *no adjustable parameters.* In this light one must conclude that the observed agreement between theory and experiment is quite satisfying. Notice that the slopes of the two lines in Fig. 5 differ markedly, in the ratio

$$\gamma_H^2[S_H(S_H+1)]^{1/2}/\gamma_D^2[S_D(S_D+1)]^{1/2}\approx 26 ,$$

indicating that the spectral width for cross relaxation is highly dependent on the strength of the S spin. However, the intercepts are essentially independent of the nonresonant spin, with a weak

$$[S_H(S_H+1)]^{1/2}/[S_D(S_D+1)]^{1/2}\approx 0.6$$

dependence. Thus for structurally equivalent systems, the ability of low-energy ($\hbar\omega_1 \rightarrow 0$) dipolar fluctuations to produce cross relaxation is not dependent on the gyromagnetic ratio characterizing the dipolar spin system. This is in sharp contrast to other relaxation mechanisms, such as relaxation by translational diffusion, where the strength of the interaction M_{IS}^2 and the correlation time τ_c are not intimately related, as they are here in the case of dipolar cross relaxation.

VI. TRANSIENTS

In this section, the early time behavior of the spin-locked ^{89}Y magnetization is discussed. Data for this regime, where the condition $t \gg \tau_c$ is not valid, has been omitted from Figs. 2 and 3 for clarity. Figure 6 displays the full time evolution of the magnetization; the early time behavior has been expanded in the inset. As is most evident, this regime is characterized[1,3,7,16,17,23–26] by large oscillations in the magnetization, which eventually damp out for $t \gg \tau_c$. These oscillations are shown for several values of H_1 in Fig. 7. Before proceeding with an analytical treatment, and in order to gain a more intuitive understanding, a description from a classical viewpoint will be posited.

Classically, the initial oscillations may be understood as resulting from the coherent precession of the spins about their local effective fields.[17,25] The situation is sketched in Fig. 8, where the local effective field H_{eff}, of some particular I spin is depicted as the vector sum of the applied field H_1 and some local field H_L. From this simple picture, the major features of the transients can be understood. First, since the local fields H_L are random in direction, the oscillation frequency must be roughly $\omega_1 = \gamma_Y H_1$, since the average spin will experience that field. Second, the oscillations will die out in a typical dephasing time $T_{2_{IS}}$ independent of H_1, since this is just a reflection of the distribution of local fields. Third, the amplitude A of the oscillations will decrease as H_1 increases relative to H_L, since the angle between H_1 and H_{eff} will decrease. Lastly, the magnetization

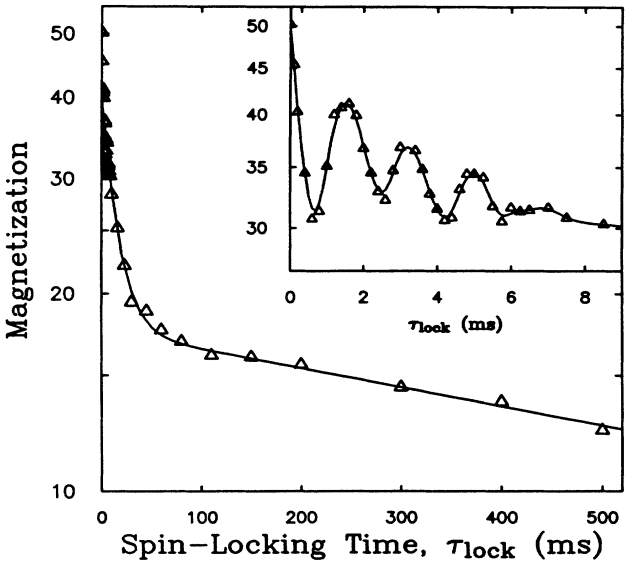

FIG. 6. Full time evolution of the spin-locked ^{89}Y magnetization in YD_2, including the transient oscillations exhibited in the early time regime. Inset is an expansion of the first few milliseconds. Solid line is a guide to the eye. Data is for $H_1 = 3$ G.

remaining parallel to H_1 after the transient oscillations have subsided, M_0', will increase as H_1 increases, for the same reason. All these qualitative observations are confirmed in the data of Fig. 7.

The transient oscillations are an indication that the initial spin-locked state is not a quasiequilibrium one. The

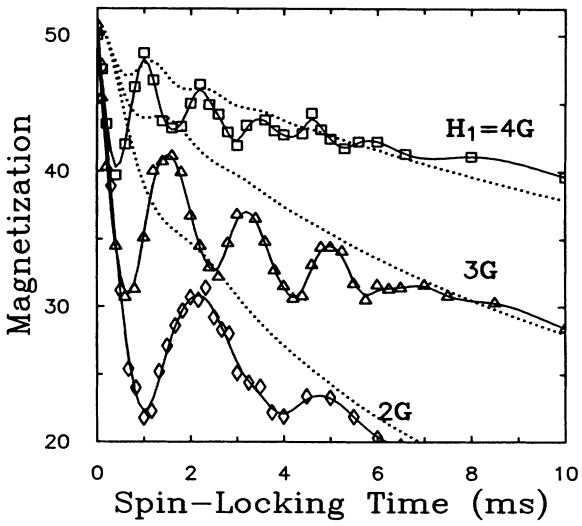

FIG. 7. Transient oscillations for three values of the rotating field H_1. Solid lines are guides to the eye. Dotted lines are from the theory of Sec. VI, exhibiting oscillations smaller than observed experimentally. The discrepancy is discussed in the text.

sudden occurrence of a new Hamiltonian brought on by spin-locking imposes a periodic time dependence on the magnetization, as is evident in Eq. (26) for $t \sim \tau_c$. The decay of the oscillations represents the establishment of a true rotating frame spin temperature, which requires a typical dephasing time $T_{2_{IS}}$ following the sudden change in Hamiltonian to occur. During the oscillations, energy is transferred back and forth between Zeeman and dipolar subsystems.[25,26] Once the oscillations have died away, the quasiequilibrium state is describable by a single spin temperature; then, the thermal mixing and eventual equilibrium, the subjects of the preceeding sections, occur.

To describe the spin system before a spin temperature has been established, note that the component of the magnetization along the applied rotating field is a well-defined quantity.[7] Utilizing energy conservation in the form

$$\langle \mathcal{H}_I(t) \rangle + \langle \mathcal{H}_S(t) \rangle = \langle \mathcal{H}_I(0) \rangle + \langle \mathcal{H}_S(0) \rangle \ , \tag{36}$$

a more general relation,[7] similar to Eq. (24), can be written using the time-dependent form of Eq. (26):

$$\frac{d}{dt}\langle \mathcal{H}_I(t) \rangle = -[(1+\epsilon)\langle \mathcal{H}_I(t) \rangle - \epsilon(\langle \mathcal{H}_S(0) \rangle + \langle \mathcal{H}_I(0) \rangle)]M_{IS}^2 \int_0^t d\tau \cos(\omega_1 \tau) C(\tau) \ . \tag{37}$$

Integrating, and using $M_I(t) = -\langle \mathcal{H}_I(t) \rangle / H_1$, one immediately obtains the general solution

$$M_I(t) = M_I(\infty) + [M_I(0) - M_I(\infty)] \exp\left[-(1+\epsilon) M_{IS}^2 \int_0^t dt' \int_0^{t'} d\tau \cos(\omega_1 \tau) C(\tau) \right] , \tag{38}$$

where $M_I(\infty)$ was given as M_f in Eq. (16). For $t \sim \tau_c$, the integral in Eq. (38) indicates that an oscillation will be superimposed upon the decaying magnetization. Equation (38) is not integrable in closed form for a Lorentzian correlation function. Therefore the integration was performed numerically using Simpson's rule for each of the three values of H_1 shown in Fig. 7. The powder average values of the parameters τ_c ($=1.003$ ms), M_{IS}^2 ($=1.145 \times 10^6$ s^{-2}), and $(\Delta H_{SS}^{(S)})^2$ ($=9.7$ G^2) calculated from the lattice sums in Secs. IV and V [Eqs. (18), (19), and (22)] were used in the integrations. These theoretical curves are plotted as dotted lines in Fig. 7. The theory agrees well with the asymptotic behavior of the oscillating decay; this is due to the cross-relaxation process already discussed and for which the theory was found quite satisfactory. However, the amplitude of the observed oscillations is much more dramatic than the slight oscillations predicted by Eq. (38). The additional coherency observed is physical in origin. It arises from the high symmetry of the YH_2 system, which has the CaF_2 structure, where the yttrium atoms form a fcc lattice[8–11] and the protons primarily reside on the tetrahedral interstitial sites,[20–22] forming a sc lattice. A given proton mutual spin flip will thus cause highly correlated field fluctuations at numerous nearby yttrium sites; since ^{89}Y is 100% abundant, this will have a coherent effect on the net yttrium magnetization. For $t \gg \tau_c$, after many proton spin flips have occurred, such correlations become unimportant due to the random nature of the spin-flip process. But for $t \sim \tau_c$, the effect is appreciable. Such enhanced coherency is *not* observed in related double-resonance experiments[3,4,24] on CaF_2 and organic compounds, since in those systems the magnetically active I-spin nuclei are dilute; ^{43}Ca and ^{13}C are only 0.13% and 1.1% abundant, respectively. In those cases, the contribution of each nucleus may indeed be considered individually; nearby mutual spin flips will produce a field fluctuation only for a single, isolated nucleus.

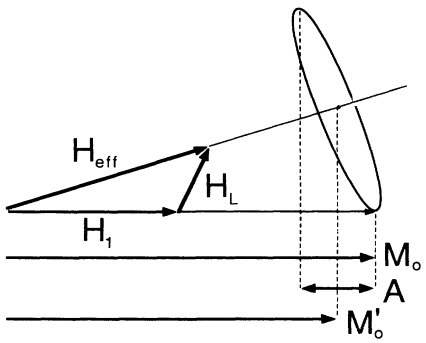

FIG. 8. Classical model for transient oscillations. The oscillation amplitude A and post-transient magnetization M_0' are related to the applied field H_1 and the local fields H_L as discussed in Sec. VI.

VII. TRANSVERSE RELAXATION

The theory discussed in the previous sections which was used to describe the time evolution of the spin-locked ^{89}Y magnetization during cross relaxation is quite general, and, indeed, is valid for $H_1 \to 0$. In that limit, it is not appropriate to discuss the magnetization in terms of cross relaxation, since with $H_1 = 0$, the rotating frame Zeeman-energy reservoir has zero heat capacity. Instead, the transverse relaxation of the freely-precessing magnetization is discussed. However, since the theory is formally equivalent, Eq. (38) may be rewritten for $H_1 = 0$ (and thus $\epsilon = 0$) in the form

$$M_I(t) = M_I(0) \exp\left[-M_{IS}^2 \int_0^t dt' \int_0^{t'} d\tau C(\tau) \right] . \tag{39}$$

An equivalent expression for the free induction decay can be obtained using an Anderson-Weiss model theory.[3,27,28] For the Lorentzian correlation function of

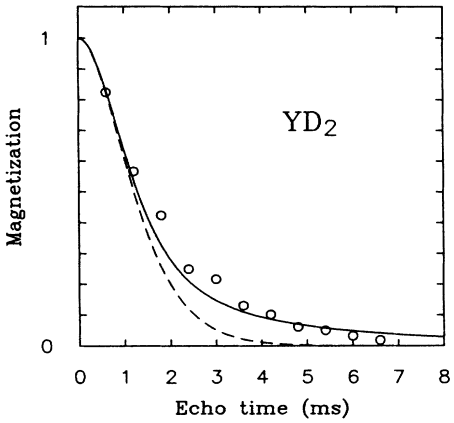

FIG. 9. Spin-echo peak magnetization as a function of echo time. Open circles are data for YD_2. Solid line is the prediction of the theory for transverse relaxation described in Sec. VII. Comparison with dashed line (same theory with naive angular average) highlights anisotropy of I-S interactions.

Eq. (30), the integration of Eq. (39) is elementary; the result is

$$M_I(t)=M_I(0)\left[1+\frac{t^2}{\tau_c^2}\right]^{M_{IS}^2\tau_c^2/2} \times \exp\left[-M_{IS}^2\tau_c t \arctan\left[\frac{t}{\tau_c}\right]\right]. \quad (40)$$

The data for the decay of the freely precessing magnetization is shown in Fig. 9. Because of an appreciable inhomogeneous broadening due to the random macroscopic fields of the small metal particles in the sample (demagnetizing fields), the free-induction decay is not indicative of the true line shape. Therefore, an ordinary Hahn spin-scho experiment was performed to obtain the shape of the true (homogeneous broadening only) free-induction decay; these data are the open circles in Fig. 9.

To compare this data with the theory just described, a powder average of Eq. (40) was performed. As in Sec. V, τ_c and M_{IS}^2 were calculated for individual crystalline directions; these provided, using Eq. (40), the contributions $m_I(t)_i$ to the total magnetization $M_I(t) = \sum_i m_I(t)_i$. The result is shown as the solid curve in Fig. 9. Considering that the theoretical curve was generated with no adjustable parameters (other than the normalizing amplitude), the agreement is quite good. The importance of careful powder averaging is demonstrated by the dashed curve in Fig. 9, which was generated by merely inserting the powder average values of the quantities M_{IS}^2 and τ_c into Eq. (40). It is readily observed that for systems where the relevant lattice sums, Eqs. (18) and (32), display appreciable anisotropy, the necessity of averaging the actual time-dependent magnetization is dictated. For the YH_2 and YD_2 (cubic) systems, one might at first assume relatively isotropic surroundings for a given nucleus. However, the $\sim 1/r^6$ dependence of the terms in Eqs. (18) and (32) enhances the discrete nature of the nearest-neighbor directions, thus producing considerable anisotropy in the summations.

VIII. SUMMARY

We have shown that the behavior of the spin-locked ^{89}Y magnetization in YH_2 and YD_2 is determined by cross relaxation between rotating-frame Zeeman- and dipolar-spin subsystems. The data obtained exhibit an exponential dependence of the cross-relaxation rate on ω_1. This behavior is adequately described in terms of the dipolar fluctuations of the nonresonant spins; calculated spectra indicate that the assumption of a Lorentzian correlation function is quantitatively valid. Additional features of the spin system, namely, Zeeman-energy–dipolar-energy equilibrium, transient oscillations, isotope effects, and transverse decay processes were examined within the same theoretical framework.

ACKNOWLEDGMENTS

A discussion with W. G. Clark early in this work has been helpful. Discussions with M. J. R. Hoch and assistance from M. J. Hirsch are appreciated. This work is supported by the National Science Foundation under Grant No. DMR-8306515.

[1]S. R. Hartmann and E. L. Hahn, Phys. Rev. **128**, 2042 (1962).
[2]F. M. Lurie and C. P. Slichter, Phys. Rev. **133**, A1108 (1964).
[3]D. A. McArthur, E. L. Hahn, and R. E. Walstedt, Phys. Rev. **188**, 609 (1969).
[4]A. Pines, M. G. Gibby, and J. S. Waugh, J. Chem. Phys. **59**, 569 (1973).
[5]H. T. Stokes and D. C. Ailion, Phys. Rev. B **15**, 1271 (1977).
[6]K. Akasaka, S. Ganapathy, C. A. McDowell, and A. Naito, J. Chem. Phys. **78**, 3567 (1983).
[7]D. E. Demco, J. Tegenfeldt, and J. S. Waugh, Phys. Rev. B **11**, 4133 (1975).
[8]A. Pebler and W. E. Wallace, J. Phys. Chem. **66**, 148 (1962).
[9]C. E. Lundin and J. P. Blackledge, J. Electrochem. Soc. **109**, 838 (1962).
[10]H. E. Flotow, D. W. Osborne, and K. Otto, J. Chem. Phys. **36**, 866 (1962).
[11]K. Dialer and B. Frank, Z. Naturforsch. B **15**, 58 (1960).
[12]M. J. Hirsch and D. F. Holcomb, Phys. Rev. B **33**, 2520 (1986).
[13]J. H. Van Vleck, J. Chem. Phys. **5**, 320 (1937).
[14]D. Wolf, *Spin-temperature and Nuclear-spin Relaxation in Matter* (Oxford University Press, Oxford, 1979).
[15]A. Abragam, *The Principles of Nuclear Magnetism* (Oxford University Press, London, 1961).

[16]J. Jeener, H. Eisendrath, and R. Van Steenwinkel, Phys. Rev. **133**, A478, (1964).
[17]P. Mansfield, K. H. B. Richards, and D. Ware, Phys. Rev. B **1**, 2048 (1979).
[18]R. Lenk, Chem. Phys. Lett. **63**, 416 (1979).
[19]J. H. Van Vleck, Phys. Rev. **74**, 1168 (1948).
[20]D. Khatamian, W. A. Kamitakahara, R. G. Barnes, and D. T. Peterson, Phys. Rev. B **21**, 2622 (1980).
[21]D. L. Anderson, R. G. Barnes, T. Y. Hwang, D. T. Peterson, and D. R. Torgeson, J. Less Comm. Met. **73**, 243 (1980).
[22]J. A. Goldstone, J. Eckert, P. M. Richards, and E. L. Venturini, Solid State Commun. **49**, 475 (1984).
[23]M. Mehring, *High Resolution NMR Spectroscopy in Solids,* Vol. 11 of *NMR, Basic Principles and Progress,* edited by P. Diehl, E. Fluck, and R. Kosfeld (Springer-Verlag, Berlin, 1976).
[24]D. L. VanderHart and A. N. Garroway, J. Chem. Phys. **71**, 2775 (1979).
[25]P. Mansfield and D. Ware, Phys. Rev. **168**, 318 (1968).
[26]J. Jeener, R. Du Bois, and P. Broekaert, Phys. Rev. **139**, A1959 (1965).
[27]M. Mehring, G. Sinning, and A. Pines, Z. Phys. B **24**, 73 (1976).
[28]P. W. Anderson and P. R. Weiss, Rev. Mod. Phys. **25**, 148 (1953).